



The interface mixing layer and the tidal dynamics at the eastern part of the Strait of Gibraltar

Jesús García Lafuente ^{a,*}, Elisa Bruque Pozas ^{a,b}, José Carlos Sánchez Garrido ^a, Gianmaria Sannino ^c, Simone Sammartino ^a

^a Physical Oceanography Group, University of Málaga-CEIMAR, Málaga, Spain

^b Laboratoire de Technologie Écologique, Ecole Polytechnique Fédérale de Lausanne (EPFL), Lausanne, Switzerland

^c ENEA, Ocean Modelling Unit, via Anguillarese 301, 00123, Rome, Italy

ARTICLE INFO

Article history:

Received 20 October 2012

Received in revised form 18 February 2013

Accepted 28 February 2013

Available online 14 March 2013

Keywords:

Numerical model

Entrainment

Internal waves

Mixing

Hydraulic control

Alboran Sea

Tides

ABSTRACT

A non-hydrostatic numerical model forced by tides has been adapted to the Strait of Gibraltar area to investigate the dynamics of the interface layer in the eastern part of the strait, namely the area that extends from the main sill of Camarinal to the eastern exit of the strait. The model reproduces the tidal oscillations of the interface thickness and the mean depth, showing that the westward barotropic tide raises the interface and reduces its thickness, thus being the physical mechanism that re-stratifies the water column. Several processes are involved in the thickening and sinking tidal phase of the interface: (1) the eastward horizontal advection from Tangier basin, located west of Camarinal sill, where the huge dissipation associated with hydraulic transitions generates a remarkable mixing layer, (2) entrainment as the interface waters progress towards the Mediterranean Sea and (3) internal friction associated with the large amplitude internal waves radiated into the Mediterranean. Some biologically-related implications of the interface dynamics are also examined.

© 2013 Elsevier B.V. All rights reserved.

1. Introduction

The mixing driven by the velocity shear and the tidal currents that interact with a constraining bathymetry invalidates the standard model of a two-layer exchange of homogeneous Mediterranean and Atlantic waters through the strait of Gibraltar. It cannot explain relevant features dealing with mixing and entrainment of water (Bray et al., 1995; García Lafuente et al., 2000) and biologically-related processes (Echevarría et al., 2002; Macías et al., 2007) and is also unable to account for observed details of the internal hydraulic of the exchange (Sannino et al., 2007, 2009).

Bray et al. (1995) included an interface mixing layer in the analysis of the exchange through Gibraltar. The layer increases its thickness away from Camarinal sill (CS, see Fig. 1) in both directions and contributes to the inflow east of CS and to the outflow west of CS. Tides were not incorporated in their conceptual model but they were in Sannino et al. (2007, 2009) and Sánchez-Garrido et al. (2011), who extended the two-layer hydraulic theory to three layers to explain the persistence of hydraulic control in key sections of the Strait that are not properly addressed in the simpler two-layer model.

Echevarría et al. (2002) analyzed the role of the interface in biological processes. They pointed out the importance of internal features like the internal hydraulic jump formed leeward of CS to supply energy for mixing and, hence, to originate and maintain the interface layer, an issue further investigated by Macías et al. (2007). Echevarría et al. (2002) showed that the depth and thickness of the interface layer have along-strait structure, being shallower at the eastern part of the Strait where the layer is associated with peak values of chlorophyll fluorescence (Macías et al. 2007), and also cross-strait structure due to planetary rotation, which cannot be ignored as the internal Rossby radius of deformation is comparable to the width of the strait. García Lafuente et al. (2000) showed that the depth and thickness of the interface layer are modulated by tides at the eastern part of the strait and Macías et al. (2006) noted a corresponding modulation of the flux of phytoplankton biomass into the Alboran Sea, which exhibits a pulsating pattern according to these authors.

From a biological point of view the upward sloping of the interface layer to the east introduces an important asymmetry between the western and eastern halves of the strait. In large areas of the eastern half the layer is shallow enough to expose its nutrient-enriched waters to solar radiation and enhance primary production. Since this layer enters the north-western sector of the Alboran Sea, it may contribute to the water enrichment there (Macías et al., 2007, 2008; Vázquez et al., 2009), although the impact of this process to the productivity of the area is a subject of ongoing research.

* Corresponding author at: Campus de Teatinos, s/n, University of Málaga, 29071 Málaga, Spain. Tel.: +34 952132721.

E-mail address: glafuente@ctima.uma.es (J. García Lafuente).

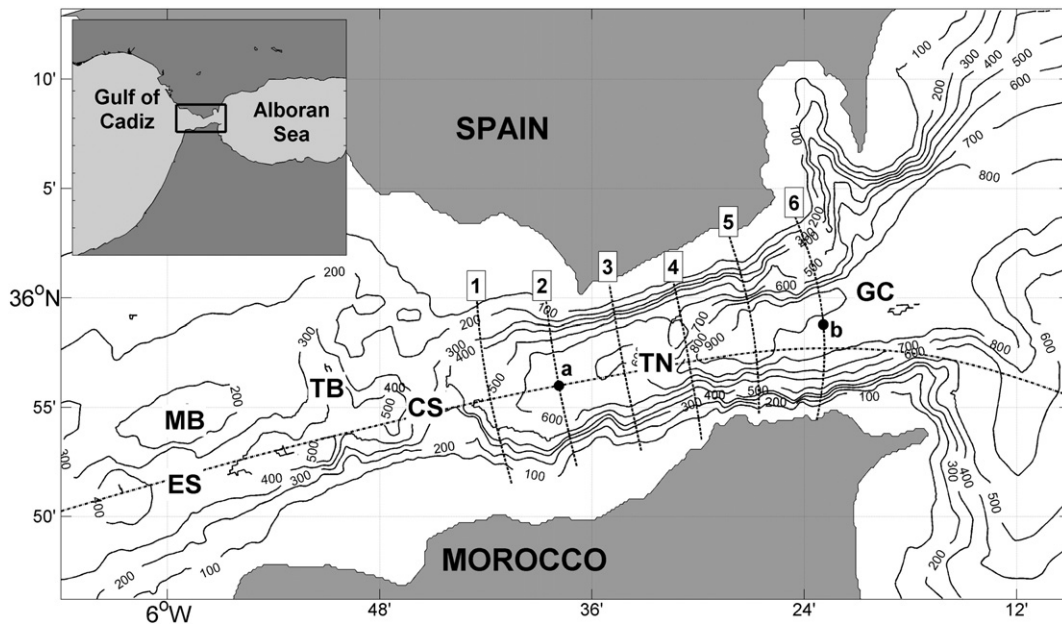


Fig. 1. Map of the Strait of Gibraltar showing the main topographic features mentioned in the text. From left to right they are: ES, Espartel Sill; MB, Majuan Bank, a pronounced seamount north of ES; TB, Tangier Basin; CS, Camarinal sill; TN, Tarifa Narrows; GC, Gibraltar–Ceuta section (eastern exit of the Strait). Labeled dashed lines are cross-sections used to carry out different computations (see text). Dot-dashed line is the along-strait main section used to present flows and other parameters in successive figures. The inset shows the two basins adjacent to the strait, the Gulf of Cadiz in the Atlantic Ocean and the Alboran Sea in the Mediterranean Sea.

From a physical point of view, the eastern half of the strait is also interesting since it is systematically swept by large-amplitude internal wave (LAIW, hereinafter) trains that originate at CS after the release of the hydraulic jump periodically formed leeward of the sill (Armi and Farmer, 1988; Sánchez-Garrido et al., 2011; Vázquez et al., 2009) and radiates finally into the Mediterranean Sea. LAIW have been linked to biological activity because of their potential for mixing and enrichment of the interface and surface layers (Macías et al., 2007, 2008; Vázquez et al., 2009). All these factors have motivated the selection of the eastern half of the strait as the target area of our study, which is carried out using the non-hydrostatic version of the Massachusetts Institute of Technology general circulation model (MITgcm, Marshall et al., 1997a,b). This model has been already used by Sánchez-Garrido et al. (2011) to reproduce successfully the generation, evolution and propagation of LAIW in the strait of Gibraltar. The objective of this paper is the comprehensive description of the dynamics of the interface layer at tidal time-scales and its likely connections with biological. The paper is organized as follows. Section 2 presents a short summary of the numerical model, Section 3 describes the spatial-temporal behavior of the interface layer in the eastern part of the strait, Section 4 addresses the different processes that contribute to the interface dynamics and Section 5 describes likely biological connections of the interface dynamics. Section 6 summarizes our conclusions.

2. Numerical model

The MITgcm solves the fully non-linear, non-hydrostatic Boussinesq equations with a spatial finite-volume discretization on a curvilinear grid. The model is described on the MITgcm Group Website (http://mitgcm.org/sealion/online_documents/node2) and in Marshall et al. (1997a,b). Details of the development of a regional model of the Strait of Gibraltar on the basis of the MITgcm source code can be seen in Sánchez-Garrido et al. (2011). A short overview is given next.

The model domain, covering part of the Alboran Sea and the Gulf of Cadiz, is horizontally discretized with using a grid with $\Delta x \sim 50$ m and $\Delta y \sim 200$ m within the Strait and 53 vertical levels

with vertical step $\Delta z \sim 7.5$ m in the upper 300 m, that gradually increases towards the bottom. The bottom topography has been obtained by merging the ETOPO2 v2 (2006) bathymetry with the high resolution bathymetric chart of the strait of Gibraltar by Sanz et al. (1991). The sub-grid scale mixing and dissipation parameterization is the same as in Sánchez-Garrido et al. (2011), which follows the turbulent closure schemes by Leith (1968) for the horizontal viscosity and Pacanowski and Philander (1981) in the vertical. The background vertical diffusivity has been set to $\kappa_b = 10^{-7} \text{m}^2 \text{s}^{-1}$ and a maximum of $\kappa = 10^{-2} \text{m}^2 \text{s}^{-1}$ has been prescribed to avoid unrealistically high values. This limit is within the upper range of values for the turbulent diffusion coefficient reported in Wesson and Gregg (1994) in the vicinity of CS. Although the Pacanowski and Philander (1981) parameterization was developed for models with vertical resolution lower than used here, it can be tuned for different regimes since it depends on dimensional constants. Actually, it has been applied satisfactorily in very high vertical resolution models (Sánchez-Garrido et al., 2011; Stashchuk and Vlasenko, 2009; Vlasenko and Stashchuk, 2007; Vlasenko et al., 2009) and more recently by Sannino et al. (2012) who showed that it provides very realistic mixing and entrainment in their high resolution, non-hydrostatic model of the strait of Gibraltar.

Initial conditions for temperature and salinity were obtained from Medar-MedAtlas Database (MEDAR Group, 2002) for the climatological month of April. The basic two-way exchange is obtained by laterally forcing the model through the imposition of mean baroclinic velocities and tracers extracted from the intermediate resolution model of Sannino et al. (2009). The model is run with this configuration for a spin-up period of 11 days, after which a quasi-steady circulation is achieved. Tidal forcing is then introduced by forcing the model laterally with the main diurnal (O1, K1) and semidiurnal (M2, S2) barotropic tidal velocities from the aforementioned model by Sannino et al. (2009) and the simulation was extended for another spin-up period of 11 days in order to attain a stable time-periodic solution. One month of this final solution constitutes the numerical dataset of this study. This same dataset has been compared successfully with observations in Sánchez-Garrido et al. (2011) in their study of LAIW in the strait of Gibraltar.

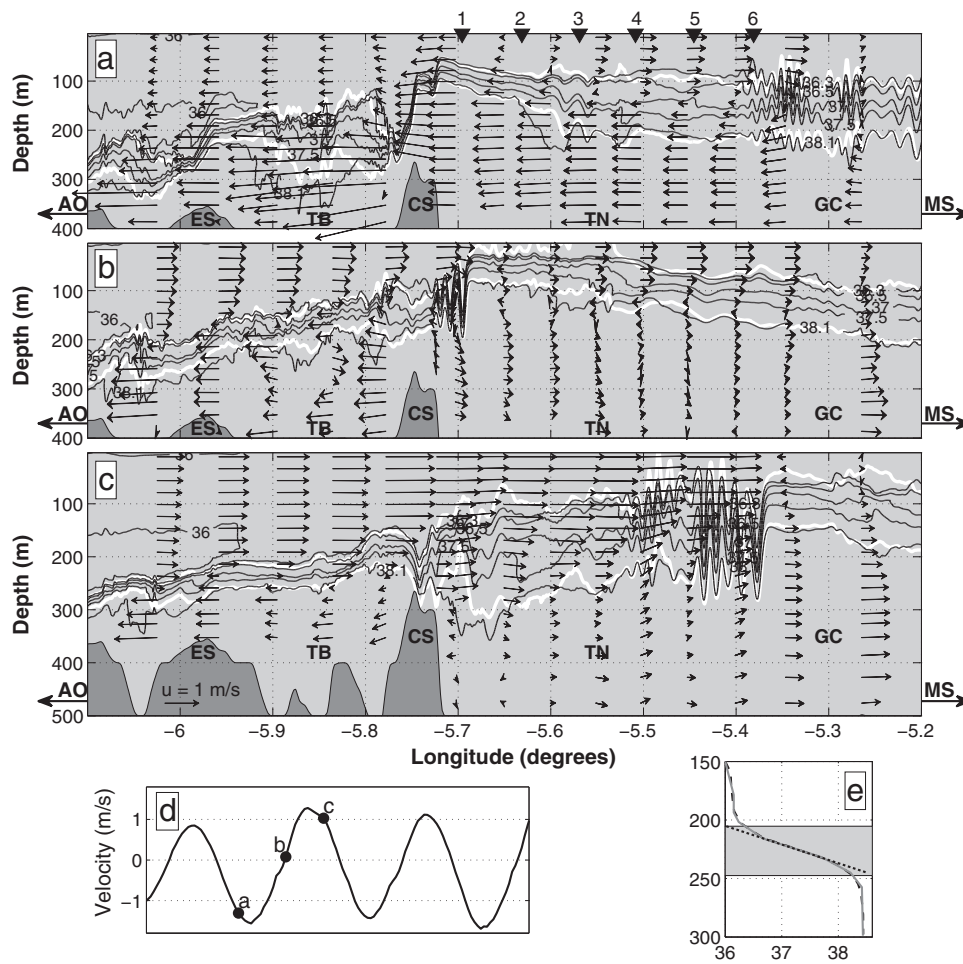


Fig. 2. Panels a), b) and c): Along-strait velocity field (velocity scale in panel c) in the along-strait section indicated in Fig. 1 at three different moments of the tidal cycle (panel d). Black lines are isohalines of $S = 36.0$ (only visible far left of the panels), 36.3 (S_A), 36.5 , 37 , 37.5 and 38.1 (S_M). Thick white lines are the boundaries of the interface layer according to the hyperbolic tangent function method explained in the text. Panel d) is the barotropic tidal current at CS section and shows the moments of the snapshots a), b) and c). Panel e) shows a salinity profile to illustrate the determination of the boundaries of the interface layer by means of the hyperbolic tangent method. Labeled inverted triangles on top of the panels indicate the location of the six cross-sections of Fig. 1. Acronyms AO and MS stand for Atlantic Ocean and Mediterranean Sea.

3. The tidal behavior of the interface layer

3.1. Definition of the interface layer thickness and depth

Salinity is the variable that makes the greatest contrast between Mediterranean and Atlantic and it is customary to select isohalines of given values to define the boundaries of the interface layer. The spatial accelerations of the exchanged flows and the mixing associated with this sheared flow make the numerical value of the bounding isohalines be spatially dependent (García Lafuente et al., 2000). For this reason, other techniques involving the fitting of vertical salinity profiles to prescribed functions have been developed to make the definition spatially independent (Bray et al., 1995; Echevarría et al., 2002; Sannino et al., 2007, 2009). The procedure described in Sannino et al. (2007, 2009) has been applied to our data to define the interface depth and thickness. The method fits the vertical profiles of salinity to a hyperbolic tangent function and the depths at which the straight line passing through the inflection point of the fitted curve intersects the vertical lines passing through the surface and bottom salinity are taken as the upper and lower boundaries, respectively, and its mean position is defined as the depth of the mid-point (see sketch in Fig. 2e).

The method provides good results when the interface layer is relatively deep, as it is the case in the western half of the strait, but it sometimes fails when the interface is thick and relatively shallow, a non-unusual situation in the eastern half we are interested in. Fig. 2a–c

is three snapshots in which the hyperbolic tangent method works suitably (except for the failure around -5.6° longitude seen in Fig. 2b) and show that the boundaries prescribed by the method in the eastern strait coincide pretty well with $S_A = 36.3$ and $S_M = 38.1$. For this reason we have defined the interface by these isohalines, which avoid the mentioned failures – and has the added value of easier visualization – and selected the isohaline $S_I = 37.2$ as a proxy for the interface depth in the eastern strait.

3.2. Semidiurnal evolution of the interface layer

Fig. 2 shows the time evolution of the interface layer along the west–east vertical section of the strait axis indicated in Fig. 1. The time of each plot, referred to the barotropic tidal current at CS, is depicted in Fig. 2d. The first panel (Fig. 2a) coincides with the peak of westward tidal current¹ and illustrates the formation of the internal hydraulic jump over CS. At this time the interface layer over and east of CS is very thin and relatively shallow, while west of CS in TB it is much deeper and noticeably thicker. This asymmetry is a recurrent feature

¹ The standing wave nature of the barotropic tide in the strait implies that barotropic tidal current is to the west from low to high water and turns to the east from high to low water (García Lafuente et al., 1990). Following the accepted convention, we will refer the west-going (east-going) phase of the barotropic tidal currents as the flood (ebb) tide/current throughout the paper.

in the strait dynamics as shown in the experimental work of Sánchez Román et al. (2012). Further east the thickness of the layer increases in the wake of the LAIW train visible at the right of the panel progressing away to the sill to the east. Fig. 2b corresponds to 1 h after the low water slack tide when the hydraulic jump has been already released and progresses eastwards while disintegrating into LAIW. The interface layer ahead the leading edge of the LAIW remains thin and unperturbed by the wave train. Fig. 2c, which corresponds to the peak of ebb current (Fig. 2d), shows the LAIW train of the previous snapshot emerging into the Mediterranean Sea and leaving a very thick and relatively deeper interface layer behind, which contrasts with the much thinner layer west of CS at this time (the already mentioned asymmetry).

Several physical processes are involved in the local shrinking and stretching of the interface layer in the eastern part of the strait sketched in Fig. 2. Internal friction in this stratified shear flow produces local mixing, the LAIW being a likely mechanism of energy supply (Moum et al., 2007a,b). Horizontal advection of mixed waters during the ebb tide is another relevant mechanism we deal with in Section 4.1. During the flood tide, Mediterranean and Atlantic waters are strongly mixed in TB in the supercritical-to-subcritical flow transition downstream of the internal jump formed over CS (Fig. 2a, Armi and Farmer, 1988; García Lafuente et al., 2011; Sánchez-Garrido et al., 2011), where Wesson and Gregg (1994) reported peak values of dissipation rates in excess of $10^{-2} \text{ W kg}^{-1}$ (orders of magnitude greater than the typical values in the interior ocean). After the release of the jump near high tide, a considerable volume of this mixed water progresses eastwards in the wake of the LAIW train. Treating the flow in terms of layers, as it is the case in the present study, the vertical exchange of mass associated with mixing can be represented as entrainment of water from the underlying and overlying layers, an approach that is further analyzed in Section 4.2.

None of these processes can re-stratify the water column and make the interface layer thinner. Fig. 3 shows that in the eastern half of the strait, the flood tide (which corresponds basically with negative values of the current at 250 m depth) is the physical process responsible for the re-stratification since both depth and thickness diminish progressively to reach their minimum by the time this current vanishes at the end of the flood phase (black dots). The process is forced by the internal hydraulics of the strait: during the flood tide the hydraulic control in CS prevents all the Mediterranean water pushed westwards by the tide from crossing the sill (Sánchez Román et al., 2012) and a considerable volume remains accumulated in the eastern half of the strait. This growing pool of Mediterranean water in turn pushes the overlying layers upwards converting kinetic into potential energy and bringing the interface layer towards the surface while reducing the thickness to its minimum, hence the good positive visual correlation observed in Fig. 3 between the two latter variables ($r^2 \sim 0.7$ at lag ~ 0 at the different sections showed in Fig. 1).

3.3. Spatial-temporal variability of the interface layer

Fig. 4a and b show the time evolution of the interface layer at sites “a” and “b” in the axis of the strait (see Fig. 1). The insets illustrate that the semidiurnal periodicity of the interface thickness is far from being sinusoidal. It exhibits spring-neap modulation being thicker and showing larger semidiurnal oscillations in spring tides. The diurnal inequality is clearly distinguishable in the neap period (days 20–27, Fig. 4c), a result that stems from the relatively high importance of diurnal tidal currents. The inequality affects the formation and release of the hydraulic jump over CS (Armi and Farmer, 1988) and, hence, the appearance of LAIW trains in the eastern strait (Sánchez Garrido et al., 2008; Watson and Robinson, 1990), which in turn influences the thickness of the interface layer (Fig. 4a and b). The interface layer shows spatial structure as well. Regardless of the fortnightly cycle, its mean thickness increases to the east, the range of semidiurnal

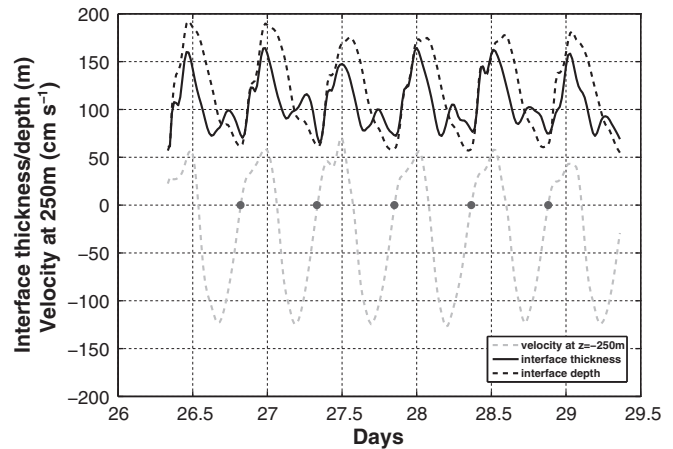


Fig. 3. Solid line: Interface thickness estimated as the vertical distance separating $S_M = 38.1$ and $S_A = 36.3$ isohalines. Black dashed line: depth of the $S_I = 37.2$, a proxy of the interface depth. Gray dashed line: along-strait velocity at 250 m depth within the Mediterranean layer. Black dots mark the zero-crossing of the current from negative (flood tide) to positive (ebb tide) and correspond approximately with the end of the flood tide. The three variables are from site “a” (Fig. 1) and have been smoothed by a Gaussian filter of cutoff frequency 1 cph in order to remove the high frequency fluctuations associated with the LAIW.

oscillations decreases and the semidiurnal periodicity blurs (compare insets in Fig. 4a and b) and it almost disappears towards the eastern end of the strait during neap-tides (Fig. 4b).

Shaded contours of Fig. 5 summarize the spatial-temporal evolution of the interface thickness along the central axis of the strait. Some of the above described features, such as the progressive thickening of the interface layer towards the east or the weakening of the semidiurnal signal, are easily identifiable. The behavior of the interface thickness downstream (to the west) of ES and CS deserves particular attention. The deep gray shading located at 5.8°W west of CS is the manifestation of the hydraulic jump or, more specifically, the supercritical-to-subcritical flow transition downstream the jump in TB. When the jump is released, the deep gray shading (thicker interface) progresses eastwards leaving a rather stratified water column (light gray) at this location (5.8°W), which eventually thickens by many meters in the next tidal cycle. On the contrary, at ES the interface thickness is within the range 50–70 m all the time and no progression to the east is observed. Notice also that the thickening of the interface in the flow transition downstream ES shows little tidal modulation as compared to the transition downstream CS. All this suggests that the hydraulic control over ES is more permanent than over CS, as put forward by Sannino et al. (2007, 2009) and Sánchez-Román et al. (2009).

The deep gray contours west and east of CS in Fig. 5 tend to be aligned along straight lines of negative and positive slopes, respectively (see white lines). In this time-space diagram the slope is indicative of the velocity at which the disturbances propagate, which is readily estimated (values beside the lines). East of the sill, three regions of different positive slope can be distinguished: the first one runs from around 5.8°W , where strong mixing takes place in the supercritical-to-subcritical flow transition, until a short distance east of CS (speed 0.3 ms^{-1}); the second one is from here to the Gibraltar–Ceuta section (GC, see Fig. 1) where the disturbance speed is around 2 ms^{-1} and the third one is eastwards of GC where the strait opens into the Alboran Sea (Fig. 1) and the speed decreases to $0.6\text{--}0.7 \text{ ms}^{-1}$. West of CS in the TB, the disturbance propagates at around -1 ms^{-1} , the negative sign meaning westwards propagation. Since all these disturbances have tidal origin, the time-space diagram confirms the fact that the strong internal tide observed in the strait of Gibraltar is generated at CS from where it radiates in both directions.

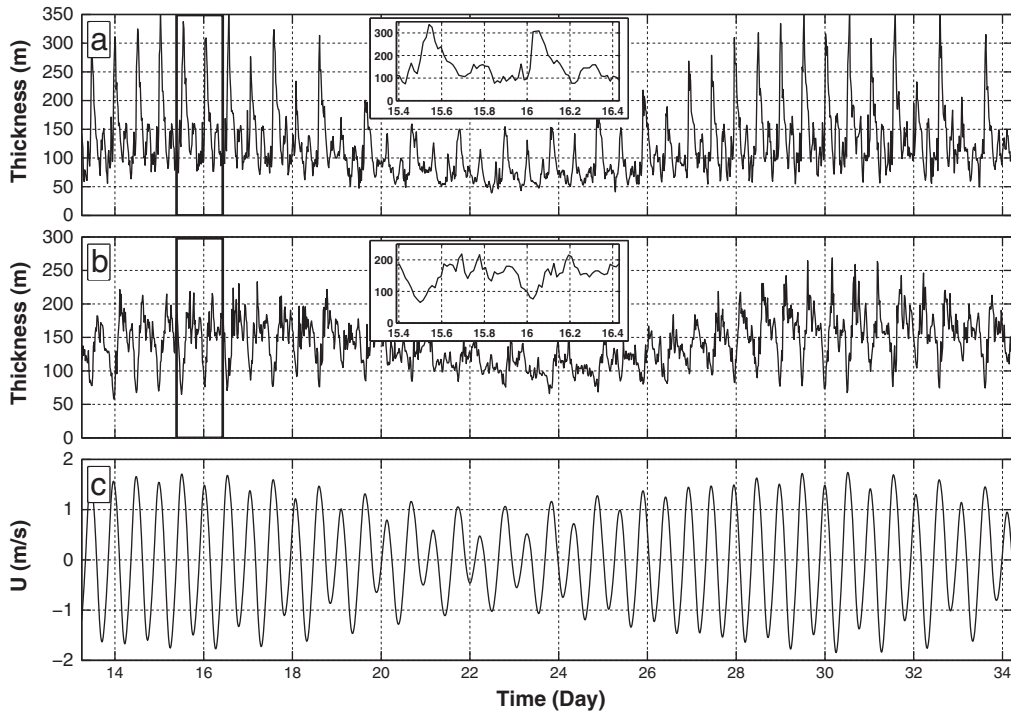


Fig. 4. Interface thickness at the sites “a” (panel a) and “b” (panel b) indicated in Fig. 1. The insets enlarge the portion of the record marked by the thick rectangles to illustrate the largely non-sinusoidal shape of the periodic oscillation, which appears more deformed to the east. Panel c) is the barotropic tidal current at CS section.

4. Processes involved in the interface dynamics

Several processes have already been invoked to explain the thickening and thinning of the interface over the barotropic tidal cycle.

4.1. Horizontal advection from Tangier basin

A passive tracer with initial concentration $C = 1$ was injected in the interface layer in TB (Fig. 6a) to assess the impact of horizontal

advection in the interface dynamics east of CS. The temporal evolution of the tracer follows the advection–diffusion equation

$$\frac{\partial C}{\partial t} = -\mathbf{u} \cdot \nabla C + \nabla \cdot k \nabla C \tag{1}$$

where C is the tracer concentration, \mathbf{u} is the velocity vector, and k is the diffusion tensor. Time origin is the slack (barotropic) tide at CS corresponding to high tide (inset in Fig. 6h). By this time the internal

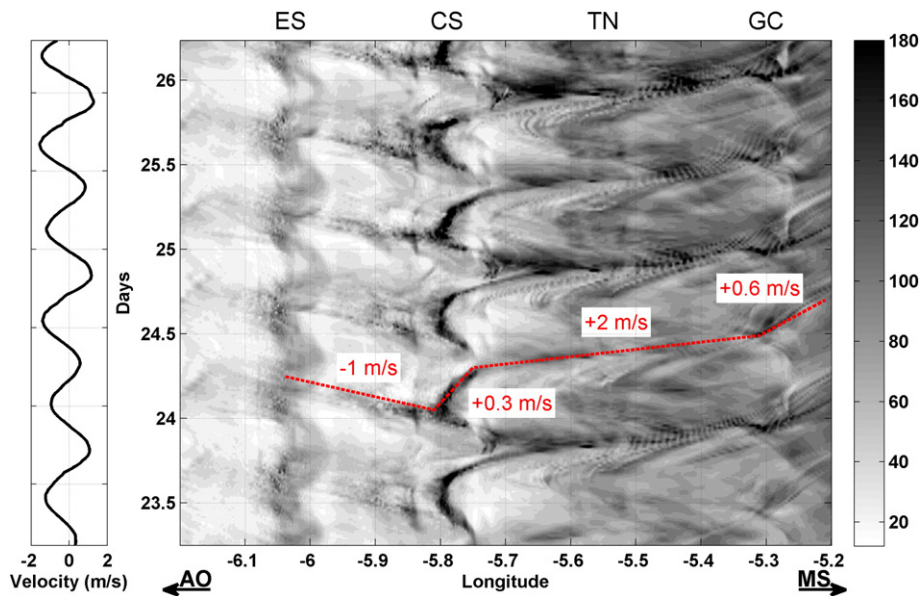
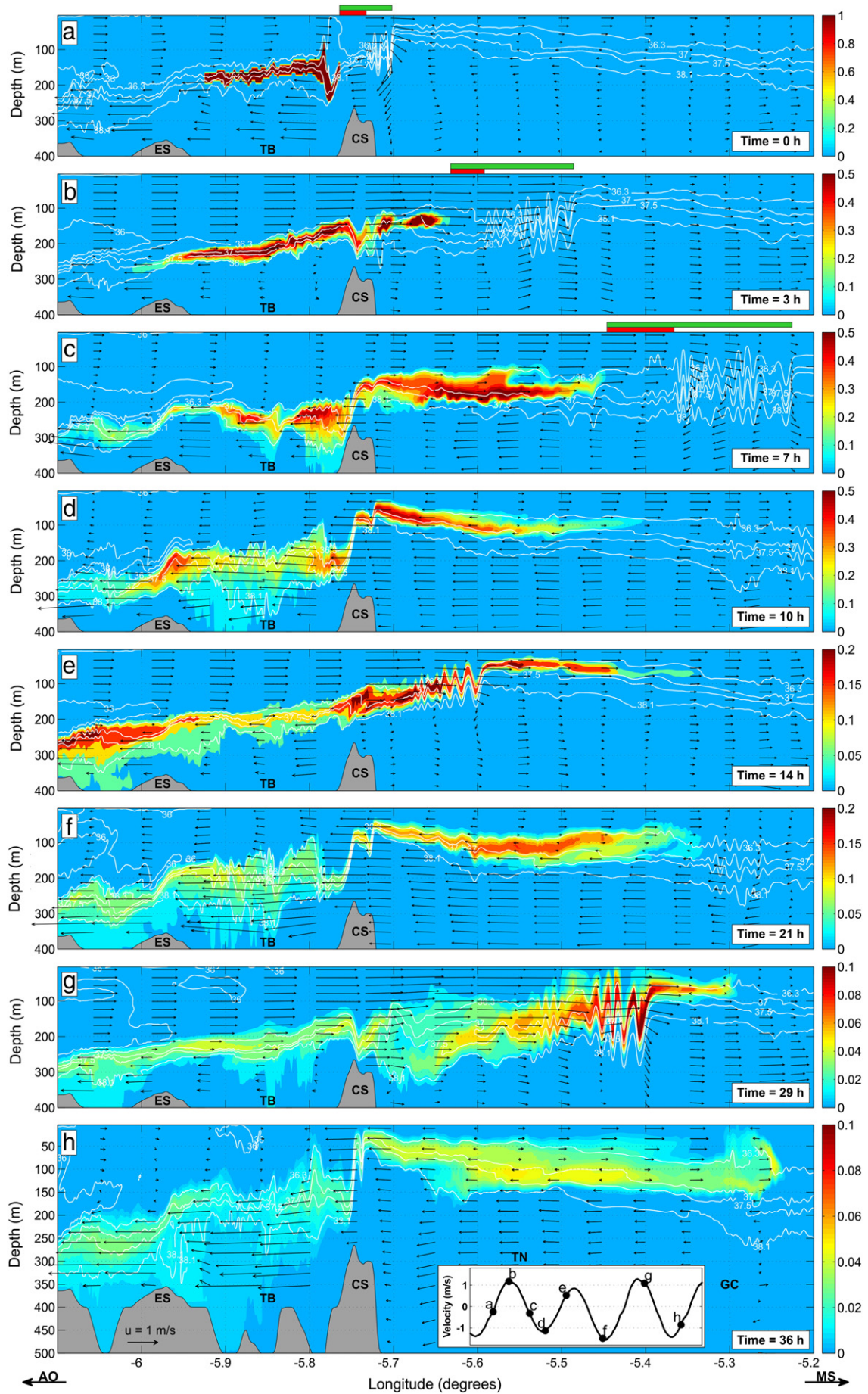


Fig. 5. Time–spatial evolution of the interface layer thickness (meters) in the along–strait section indicated in Fig. 1. The section extends over the western half of the strait where isohalines $S_A = 36.3$ and $S_M = 38.1$ are not good boundaries of the interface; for this reason the hyperbolic tangent function method has been used to estimate the interface thickness in this plot. Labels on the top indicate the main topographic features. The straight dashed lines and the numbers beside specify the propagation speed of the layer thickness, which changes from one region to the other. Barotropic tidal current at CS is shown in the left panel.



hydraulic jump has already been released (it does ~2 h before high tide) and the bore has moved ~6 km eastward of CS (green bar on top of panel 6a) showing up an incipient LAIW train behind.

During the ebb tide (Fig. 6a to c) the leading edge of the mixed water advected from TB is left behind the front of LAIW by an increasing distance (green bars on top of the panels). The relative speed is ~0.75 m s⁻¹ between t = 0 h and t = 3 h (Fig. 6a–b), and ~0.65 m s⁻¹ between t = 3 h and t = 7 h (Fig. 6b–c). The rear end of the LAIW train moves at roughly half that relative speed (~0.3 m s⁻¹, see red bars on top of the panels) due to the continuous generation of new waves (Sánchez-Garrido et al., 2011; Vlasenko et al., 2009), which increases the train length as it proceeds to the east. When the LAIW pass by, they leave behind a thickened interface and the water advected eastward from TB meets a thicker interface ahead (Fig. 6b and c). The process closely resembles the formation and evolution of LAIW ahead a buoyant river plume in the Pacific continental shelf off Oregon described by Nash and Moum (2005), who summarized the sequence as a frontal growth associated with a supercritical plume that ensues wave fission when the plume becomes subcritical and, finally, freely propagating waves. The resemblance is achieved considering a reference frame moving with the Mediterranean layer. Within this frame, the hydraulic jump formed downstream of CS during the flood tide would play the role of the supercritical buoyant plume that becomes subcritical when the internal bore is released (in the stationary reference frame). The wave fission ensues and the generated LAIW train propagates freely, leaving increasingly behind the leading edge of the plume (i.e., the advected water from CS), which would meet a thickened interface ahead.

During the flood tide (Fig. 6d) the advection is partly stopped, some water in the interface is forced oceanwards while the interface itself shallows and becomes thinner (re-stratification). Fig. 6e to h show the further evolution of the tracer remains injected at t = 0 that has not left the strait yet (no new tracer was injected in TB in the successive two tidal cycles). The pale green-yellow colors extending across the interface layer in Fig. 6g and h (note the different color scale in these panels) suggest diapycnal diffusion and this fact along with the thickening of the interface between the nose of the passive tracer and the rear of the LAIW discussed above indicates that water advection from TB cannot be the only mechanism acting to thicken the interface.

4.2. Entrainment

The sketch of Fig. 7a illustrates the procedure followed to estimate the entrained water. It represents a finite volume *V* bounded by fixed cross-strait sections, which will be eventually identify with the sections in Fig. 1, and by the two bounding interface isohalines *S_A* = 36.3 and *S_M* = 38.1.

Continuity and salt conservation equations in this control volume are written as

$$\frac{dV}{dt} = \sum_k Q_k \quad (2 - a)$$

$$\frac{dS}{dt} = \sum_k QS_k \quad (3 - a)$$

where *Q_k* and *QS_k* are the net flow and salt flux into the control volume, respectively, and *V* and *S* are the water volume and salt content in the interior. These equations are nothing but the integrated version

of volume and mass (salt in this case) equations often used in layered models (see Gerdes et al. (2002) for instance).

At tidal time-scale the isohalines are forced to undertake large vertical oscillations, implying large fluctuations of *V* and *S* and of their time derivatives. Fig. 7b shows the time evolution of *Q₂(t)* and *Q₃(t)* and their difference, which is the major contributor to *dV/dt* in Eq. (2-a) since vertical advection must be much less than horizontal advection. The difference shows a noticeable tidal periodicity indicative of the periodic thickening and slimming of the interface layer, which is also evidenced by the solid line in Fig. 3. In the long term however (i.e., averaging over several tidal cycles) the interface thickness must be locally stationary and, therefore, *dV/dt* = *dS/dt* = 0. The time average of Eqs. (2-a) and (2-b) thus reduces to (using the convention of Fig. 7a)

$$Q_{i+1} - Q_i = QA_{ei} + QM_{ei} \quad (2 - b)$$

$$QS_{i+1} - QS_i = QAS_i + QMS_i \quad (3 - b)$$

where *Q_i* is the interface layer flow through section *i* computed from the model output, *QA_{ei}* and *QM_{ei}* are the flows of entrained water from the upper (Atlantic) and lower (Mediterranean) layers that enters (positive) or exits (negative) the control volume between sections *i* and *i* + 1, *QS_i* is the salinity transport through section *i* computed from the model, and *QAS_i* and *QMS_i* are the salinity transport across the upper and lower boundaries associated with the entrained flows. They can be approached by

$$QAS_i = QA_{ei}S_A, QMS_i = QM_{ei}S_M \quad (4)$$

where *S_A* = 36.3 and *S_M* = 38.1 are the salinities of the upper and lower isohalines of the control volume. From Eqs. (2-b), (3-b) and (4), entrained flows are

$$QA_{ei} = \frac{(Q_{i+1} - Q_i)S_M - (QS_{i+1} - QS_i)}{S_M - S_A} \quad (5)$$

$$QM_{ei} = \frac{(QS_{i+1} - QS_i) - (Q_{i+1} - Q_i)S_A}{S_M - S_A} \quad (6)$$

Fig. 7c shows *QA_{ei}* and *QM_{ei}* in the 5 boxes defined by the six cross-strait sections of Fig. 1. Water entrained from above, *QA_{ei}*, is rather similar in the different boxes (around 0.025 Sv/box, light gray triangles in Fig. 7c) while *QM_{ei}* is less homogeneous, showing negative values in box 1 and also, although nearly zero, in box 4 (inverted triangles in Fig. 7c–d). The negative value of box 1 is associated with the prevailing westward flow (on average) at the lower part of the interface layer in the vicinity of CS due to the spatial acceleration of the Mediterranean layer as it approaches the sill.

More interesting is the cumulated entrained water shown by the thick triangles: in both cases it contributes positively to increase the flow through the interface layer between Sections 1 and 6. The contribution of the upper Atlantic layer is about twice that of the lower Mediterranean layer suggesting that the progressive thickening of the interface to the east is mainly due to the incorporation of fresher water from the surface layer.

Fig. 7d is the scatter plot of the entrained water versus the vertical shear. The shear in the upper boundary of the interface layer has been computed as the velocity difference between *z* = 3 m (the surface level) and the depth of *S* = 36.8 divided by the variable depth difference between both levels. Similarly, the velocity difference between *S* = 37.7 and *z* = 250 m divided by the distance between these

Fig. 6. Evolution of the passive tracer concentration injected in TB at t = 0 (panel a). White lines are *S* = 36 (only visible in the Atlantic Ocean side), *S_A* = 36.3, *S* = 37, *S* = 37.5, *S_M* = 38.1. Arrows indicate the along-strait velocity (scale in panel h). Inset in panel h) illustrates the barotropic tidal current in each panel. Green and red rectangles on top of panels a), b), and c) indicate the distance between the leading edge of the tracer and the front and rear of the LAIW train, respectively. Notice the scale changes from panels d) to e) and, again, from g) to h).

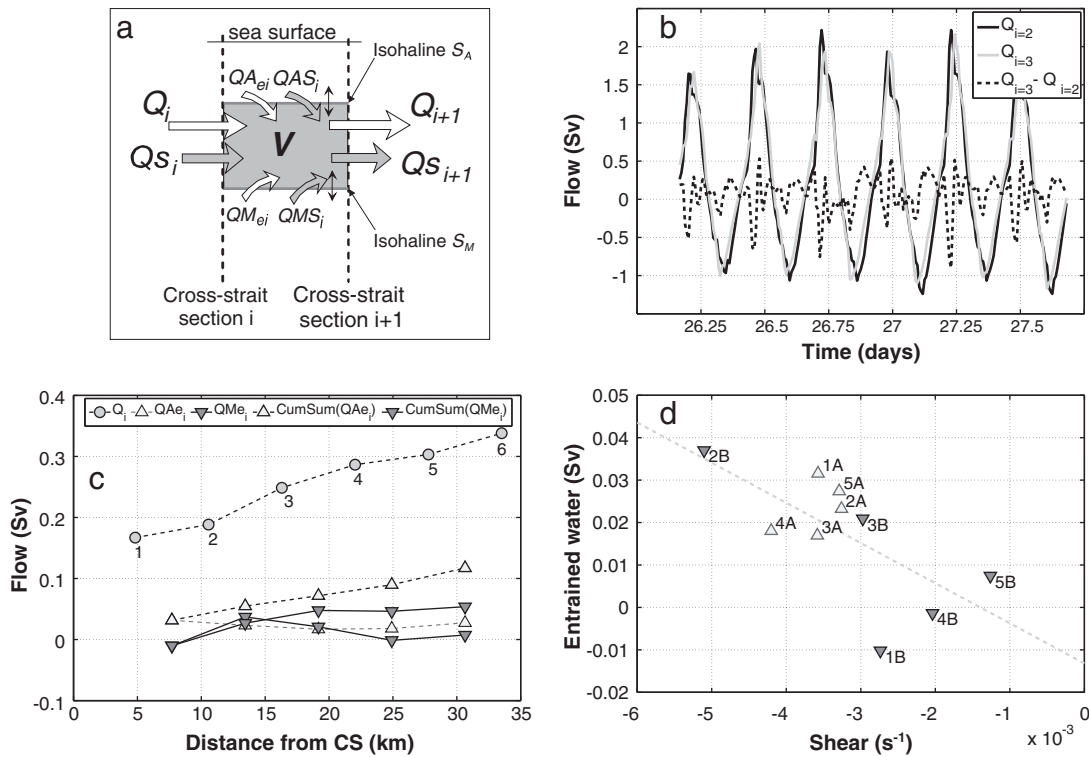


Fig. 7. a) Sketch of the volume control used to estimate the entrained water into the interface layer. Cross-strait sections that close the volume laterally will be identified with the sections shown in Fig. 1. b) Instantaneous interface flow through vertical cross-sections $i = 2$ and $i = 3$ and their difference, which is indicative of the rate of volume change dV/dt in the box defined by these sections. c) Tide-average flow through the six cross-sections of Fig. 1 (filled circles), locally entrained water from above (QAe_i , light gray triangles) and below (QMe_i , light gray, inverted triangles) and cumulated entrained water from above (black triangles) and below (black inverted triangles). d) Scatter plot of entrained water versus mean vertical shear (see text). Open and inverted filled triangles correspond to water entrained from above and below (i.e., QAe_i and QMe_i), respectively. Labels beside symbols indicate the different boxes ($i = 1, 2, \dots, 5$) for water entrained from above (A) or below (B). The straight dashed line is the linear fitting whose slope is $-9.5 \text{ Sv} \cdot \text{s}$.

levels has been used as an indicative of the shear at the lower boundary of the interface. Except for the water entrained through the bottom boundary of box 1 (symbol 1B in Fig. 7d) the rest of the dots lay close to the fitting line, suggesting the linear relationship between entrainment and shear in layered models (Gerdes et al., 2002; Nielsen et al., 2004). The unexpected position of dot 1B is due to the proximity of box 1 to CS that makes a portion of the lower part of the interface within this box be moving to the west, which implies negative entrainment as mentioned above.

4.3. Mixing by internal waves

Fig. 8 shows the salinity profiles at sites “a” and “b” of Fig. 1 after the LAIW train has passed by. The vertical salinity gradient is smoother at “b” suggesting that the halocline (and hence the pycnocline) is more eroded as the thickening of the interface progresses eastwards. Water entrainment explains partially the erosion but the mechanism acts preferably near the top and bottom of the interface layer and would leave the middle part rather unaltered. Fig. 8, however, shows that this does not seem to be the case.

In the interface layer interior, mixing would be better represented by internal friction to which the progressing LAIW trains are a potential source of energy. Left panels of Fig. 9 depict three situations of the generation and propagation of LAIWs whereas right panels present the gradient Richardson number Ri computed at 160 m depth, which is roughly the depth of the middle part of the interface layer as suggested by Fig. 8. Notice that, in the Pacanowski and Philander (1981) formulation, Ri and the turbulent diffusion coefficient are inversely related and, consequently, regions with low Ri in Fig. 9 correspond to regions with high turbulent diffusion and mixing. Very low values of Ri are found at the rear part of the progressing LAIW train, revealing favorable conditions for shear instabilities and supporting the hypothesis

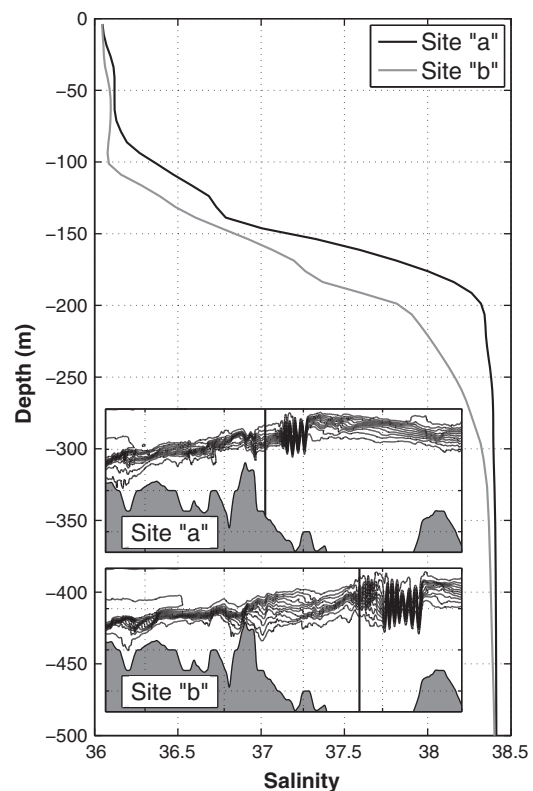


Fig. 8. Salinity profiles at sites “a” (black line) and “b” (gray line) shortly after the local passing of the LAIW train, as indicated by the vertical lines in the insets. Salinity gradient is smoother at site “b” suggesting the direct effect of the LAIW train on mixing.

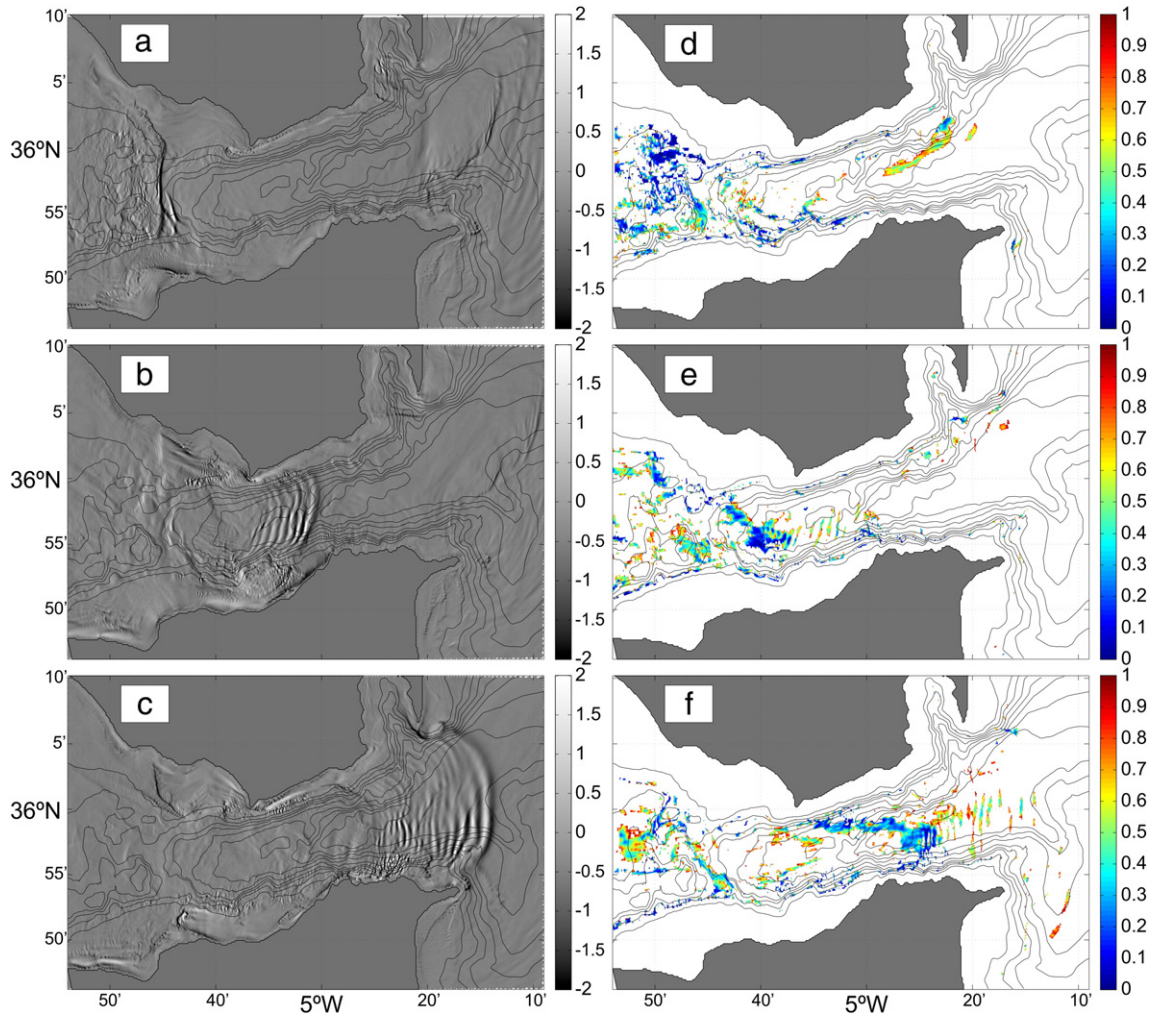


Fig. 9. Left panels: three different moments of the generation and propagation of LAIWs, which are depicted by the divergence of the surface velocity (gray scale, units of 10^{-3} s^{-1}). Panel a) shows the signature of the internal hydraulic jump downstream of CS, and panels b) and c) show the LAIW train passing off Tarifa and about leaving the Strait, respectively, after the release of the jump. Right panels: Richardson Ri number computed at 160 m depth at the same moment as in the corresponding left panel. Notice the very low values at the rear of the LAIW packet in panels e) and f) and the extended low values all over TB in panel d) coinciding with the formation of the hydraulic jump.

that LAIWs contribute to the mixing in the interior of the layer. This mechanism for mixing has been reported to occur over the Pacific continental shelf off Oregon, where LAIWs are a recurrent feature as well (Moum et al., 2007a,b). It is interesting to remark the extended very low values of Ri computed in TB in Fig. 9d. At this time no LAIWs are observed in the area and the roughness of the sea surface over and west of CS (Fig. 9a) is the only noticeable signature of the internal dynamics, which reflects the formation of the hydraulic jump in TB that is accompanied by strong mixing in the basin.

5. Biological connections of the interface dynamics

The previous section has discussed some mechanisms associated with the tidal dynamics through which the interface layer in the target area might be nutrient-enriched and brought up to the photic layer periodically. Some of them have implications on the biological productivity and deserve a more detailed analysis and discussion.

5.1. Horizontal advection

Horizontal advection is important in the interface dynamics. The huge mixing in TB during the flood tide (Fig. 9d) makes the mixed and nutrient enriched waters available for eastwards advection during the ebb tide. The TB is in the mid-channel zone of the strait

and this advection mainly involves water from this zone, which is away from the coast. The possibility however exists that enriched waters from coastal areas are injected into the main channel of the strait, as hypothesized by Vázquez et al. (2009) and Bartual et al. (2011), and contribute to the enrichment of the interface layer and the inflow.

A new experiment was carried out to address this point. Passive tracer was injected with homogeneous concentration in the middle part and in the coastal areas of the strait as shown in Fig. 10a and e, respectively. The experiment started ($t = 0$) shortly before the slack-tide corresponding to high tide (bottom panel of Fig. 10), when the hydraulic jump is about being released, and then run for 36 h. The time origin has been intentionally selected at this moment since it coincides with the beginning of the remarkable horizontal advection of interface waters to the east (Section 4.1, Fig. 6). Panels in Fig. 10 show the evolution of the vertically integrated concentration for the initial situations depicted in Fig. 10a and e.

The tracer released in the mid-channel within TB (Fig. 10a) is advected in both directions by the joint action of the mean exchange and the tidal forcing. It quickly adopts an elongated shape that outlines the main axis of the channel without intruding the coastal areas (Fig. 10b to d) and, at the end, it flows out through both open boundaries of the basin. The west-going branch flows at depths greater than the height of the MB seamount (Fig. 1), which is clearly shaped in

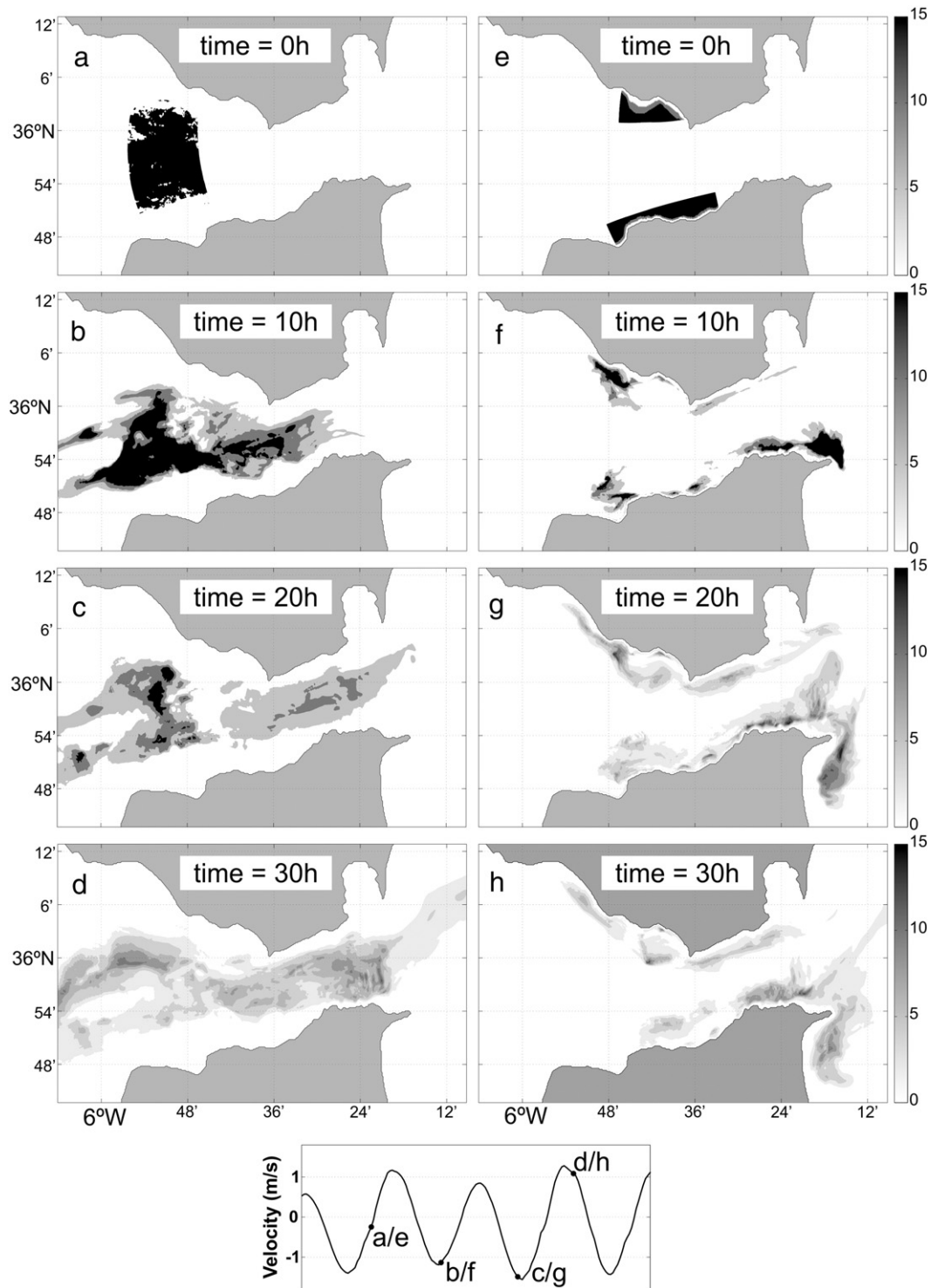


Fig. 10. Time evolution of a passive tracer injected initially ($t = 0$) at the central part of the strait in TB (panel a) and in coastal waters (panel e). Panels b) to d) show the evolution of the vertically integrated concentration at $t = 10$ h, 20 h, and 30 h, respectively, for the initial situation of panel a). Panels f) to h) do the same for the initial situation showed in e). The bottom panel is the barotropic tidal current at CS and indicates the instants of the different snapshots.

Fig. 10b–d as the outflowing water splits to skirt its pronounced topography. The branch flowing east remains basically in the central part of the channel although it approaches the shores as the strait narrows. Finally, it enters the Alborán Sea following an expected east-northeast oriented trajectory (Fig. 10c and d).

The coastal waters initially in the north (Fig. 10e) are advected in both directions by the changing tide but remain attached to the shore (Fig. 10f to h). Cross-strait injection into the main channel, if any, is negligible. The evolution of the coastal waters located initially in the

south exhibit two remarkable differences: they are advected eastwards mostly (Fig. 10g, h) and a non-negligible fraction detaches from the shore, reaching the middle channel near the eastern end of the strait (Fig. 10g) where it joins the waters flowing along the main channel (Fig. 10d). Therefore they contribute to the tracer advection towards the interior of the Alborán Sea although most of the original waters turn right as they exit the strait and remain close to the African shore (Fig. 10h), featuring a spatial pattern that closely resembles the MERIS image of Fig. 2 in Vázquez et al. (2009).

5.2. Residence time

The former experiment has shown that the mixed water in the interface layer in TB leaves the strait through both open boundaries, but it takes some time to do it. Fig. 11 presents the evolution of the tracer percentage and shows that, after 36 h (~three tidal cycles), around 60% has flowed out of TB to the Atlantic ocean through ES, 30% has already crossed CS to the east (Mediterranean) and as little as 10% still remains in the basin. Notice that the very initial partition of the percentages depends on the time origin of the experiment: the quick increase of the percentage of tracer going to the Mediterranean Sea observed in Fig. 11 follows the fact that $t = 0$ nearly coincides with the beginning of the ebb current (bottom panel of Fig. 10). Later on the percentage decreases and oscillates slightly around the mentioned value of 30%.

While the mixed waters flowing west are too much deep to contribute to the primary production (depths > 200 m, see Fig. 6), the interfacial waters flowing eastwards are inside a shallower layer within the reach of the sun radiation. In addition, they are brought closer to the surface periodically by the tidal dynamics, increasing their potential to support local primary production. The time that the interface waters mixed in TB by the hydraulic jump spend between CS and the eastern exit of the strait is not easy to determine because of the vertical shear of the currents and the low frequency tidal variability (spring-neap cycle). Judging from panels in Figs. 6 and 10, it could be estimated between two and three tidal cycles, but the interval may be longer.

6. Conclusions

The tidal dynamics of the interface layer in the eastern part of the strait shows a complex pattern that involves different physical processes. The thickness and depth of the interface have been used to analyze their periodic evolution since both variables exhibit tidal variability (Echevarría et al., 2002; García Lafuente et al., 2000). The thickening phase begins with the release of the internal hydraulic jump formed over CS during the flood tide, which indicates that horizontal advection is a fundamental ingredient of the interface dynamics, although it is not the only one. Actually, the water advection, the LAIW train generation and the thickening of the interface ahead the leading edge of the advected water are different aspects of the same process, which has clear resemblance in the dynamic of supercritical buoyant plumes found in other parts of the world (Nash and Moum, 2005; Stashchuk and Vlasenko, 2009).

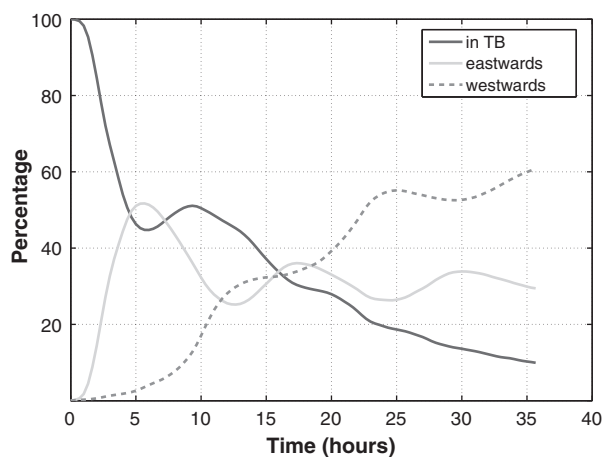


Fig. 11. Time evolution of tracer concentration (percentage). Black line is the tracer that remains in Tangier basin, gray solid and dashed lines represent the tracer advected eastwards over CS and westwards over ES, respectively.

The simple budget computation illustrated in Fig. 7a shows that tide-average water entrainment from the overlying (Atlantic) and underlying (Mediterranean) layers increases the volume transport within the interface layer in the eastern strait by a factor of 2 (Fig. 7b), of which 2/3 is entrained from above and 1/3 from below. Since nutrient source is the deep ocean, entrainment is of limited relevance in order to enrich the interface in the eastern part of the strait. Entrainment would erode the salinity (hence density) vertical gradient of the interface but the low values of the Richardson number found in the rear of the LAIW train (Fig. 9) around the midpoint of the interface layer suggest that internal friction driven by internal waves contribute noticeably to the diapycnal mixing in the interface interior.

The above processes act together to thicken the interface but none of them can explain its periodic thinning. It is the tidal current in the Mediterranean layer at the eastern strait interacting with the topographical and hydraulic constriction imposed by CS that raises and makes the interface thinner during the flood (westward) tidal phase (Fig. 3), forcing the pre-existing interface water to move towards both ends of the strait. Thus interface water must enter the Alborán Sea as successive periodic pulses modulated by tides in a manner that recalls the pulsating events cited by Macías et al. (2006).

Numerical experiments aimed to investigate biologically-related issues have been performed to address the question raised by previous studies (Bartual et al., 2011; Vázquez et al., 2009) about the possible injection of coastal waters into the main vein of the Atlantic inflow, which would contribute to its biological enrichment. Our results (Fig. 10) indicate that, to a limited extent, such injection could take place from the south but not from the north where the tracer remains attached to the shore until it enters the Alborán Sea.

The same numerical experiment was used to estimate the time that interface waters reside within the strait dimensions, which is relevant since in the eastern strait the interface is at the reach of the photosynthetic active radiation making feasible the local primary production. The time was estimated in 2–3 tidal cycles after the mixed and nutrient-enriched waters in TB are released by the loss of the hydraulic control at CS. This relatively small residence time will be further diminished by the fraction corresponding to nighttime and by the eventual deepening of the interface beyond suitable radiation levels, all which suggests that local primary production, if any, must be very limited. To this respect, some MERIS images showing cross-strait oriented bands of chlorophyll that outline the internal wave fronts (see Fig. 2 of Vázquez et al. (2009), for instance), would lead to the misleading conclusion of local primary production associated with LAIW. More likely is that chlorophyll in the observed bands had been advected from TB during a previous tidal cycle and the observed pattern is the result of its redistribution by the velocity field of the LAIW train formed during the next cycle in the manner illustrated by Fig. 6g.

Another indirect but yet interesting conclusion from this experiment is the sharing of interface waters between inflow and outflow. TB is the key place for sustained mixing to feed the interface. The mixed waters are then drained eastwards and westwards flowing across the main sills that bound the basin. Fig. 11 suggests that the sharing is in the proportion 2:1 for the outflow, indicating that the interface layer generated in TB is mainly evacuated by the outflow, a result that agrees with Bray et al. (1995) conclusions that the interface layer to the west of CS flows mainly towards the Atlantic Ocean. The incorporation of this mixed water to the outflow represents the first step of the erosion of Mediterranean waters in the Atlantic Ocean, erosion that is already distinguishable in ES, as shown by García Lafuente et al. (2011).

The model does not include the wind stress at the surface water nor the remote forcing driven by atmospheric pressure variations over the Mediterranean Sea (García Lafuente et al., 2002a,b), which are important agents to distort the periodic tidal pattern (Vázquez et al., 2008) and, hence, to affect some of our conclusions. Among

them, one particularly sensitive is the injection of coastal waters into the center of the channel, where they can be easily displaced by cross-strait Ekman transport, explaining the presence in the middle channel of chlorophyll with the same characteristics as coastal chlorophyll that was found by Macías et al. (2008).

Acknowledgments

This work is a contribution to the Spanish funded National Project INGRES 3 (CTM2010-21229-C02) and MEDEX (European MarinERA RTD activities, Project 189561) under AC CTM-2008-04150E. Partial financial support from CTM2009-05810/E (Spanish Ministry of Science and Innovation) and Project P08-RNM-3738 from Plan Andaluz de Investigación are also acknowledged. We are grateful to CRESCO Supercomputing Facilities at ENEA (www.cresco.enea.it) and to the Supercomputing and Bioinformatics (SCBI) Center of the University of Malaga. This is the publication no. 19 from CEIMAR Publication Series.

References

- Armi, L., Farmer, D.M., 1988. The flow of Atlantic Water through the Strait of Gibraltar. *Prog. Oceanogr.* 21 (1), 1–105.
- Bartual, A., Macías, D., Gutierrez-Rodríguez, A., García, C.M., Echevarría, F., 2011. Transient pulses of primary production generated by oscillatory processes in the western sector of the Strait of Gibraltar. *J. Mar. Syst.* 87, 25–36. <http://dx.doi.org/10.1016/j.jmarsys.2011.02.021>.
- Bray, N.A., Ochoa, J., Kinder, T.H., 1995. The role of interface in exchange through the Strait of Gibraltar. *J. Geophys. Res.* 100 (C6), 10755–10776.
- Echevarría, F., García Lafuente, J., Bruno, M., Gorsky, G., Goux, M., González, N., García, C.M., Gómez, F., Vargas, J.M., Picheral, M., Striby, L., Varela, M., Alonso, J.J., Reul, A., Cozar, A., Prieto, L., Sarhan, T., Plaza, F., Jiménez-Gómez, F., 2002. Physical-biological coupling in the Strait of Gibraltar. *Deep-Sea Res.* 49, 4115–4130.
- ETOPO2v2 Global Gridded 2-minute Database, National Geophysical Data Center, National Oceanic and Atmospheric Administration, U.S. Dept. of Commerce, 2006. <http://www.ngdc.noaa.gov/mgg/global/etopo2.html>.
- García Lafuente, J., Almazan, J.L., Fernandez-Castillejo, F., Kribeche, A., Hakimi, A., 1990. Sea level in the Strait of Gibraltar: tides. *Int. Hydrogr. Rev.* LXVII (1), 111–130.
- García Lafuente, J., Vargas, J.M., Plaza, F., Sarhan, T., Candela, J., Bashech, B., 2000. Tide at the eastern section of the Strait of Gibraltar. *J. Geophys. Res.* 105, 14197–14213. <http://dx.doi.org/10.1029/2000JC900007>.
- García Lafuente, J., Delgado, J., Criado-Aldeanueva, F., 2002a. Inflow interruption by meteorological forcing in the Strait of Gibraltar. *Geophys. Res. Lett.* 29 (19), 1914. <http://dx.doi.org/10.1029/2002GL015446>.
- García Lafuente, J., Alvarez Fanjul, E., Vargas, J.M., Ratsimandresy, A.W., 2002b. Subinertial variability in the flow through the Strait of Gibraltar. *J. Geophys. Res.* 107 (C10), 3168. <http://dx.doi.org/10.1029/2001JC001104>.
- García Lafuente, J., Sánchez-Román, A., Naranjo, C., Sánchez-Garrido, J.C., 2011. The very first transformation of the Mediterranean outflow in the Strait of Gibraltar. *J. Geophys. Res.* 116, C07010. <http://dx.doi.org/10.1029/2011JC006967>.
- Gerdes, F., Garrett, C., Farmer, D., 2002. On internal hydraulics with entrainment. *J. Phys. Oceanogr.* 32, 1106–1111.
- Leith, C.E., 1968. Diffusion approximation for two-dimensional turbulence. *Phys. Fluids* 10, 1409–1416.
- Macías, D., García, C.M., Echevarría, F., Vázquez-Escobar, A., Bruno, M., 2006. Tidal induced variability of mixing processes on Camarinal Sill (Strait of Gibraltar). A pulsating event. *J. Mar. Syst.* 60, 177–192. <http://dx.doi.org/10.1016/j.jmarsys.2005.12.003>.
- Macías, D., Martín, A.P., García Lafuente, J., García, C.M., Yool, A., Bruno, M., Vázquez, A., Izquierdo, A., Sein, D., Echevarría, F., 2007. An analysis of mixing and biogeochemical effects induced by tides on the Atlantic-Mediterranean flow in the Strait of Gibraltar through a physical-biological coupled model. *Prog. Oceanogr.* 74, 252–272. <http://dx.doi.org/10.1016/j.pocean.2007.04.006>.
- Macías, D., Lubian, L.M., Echevarría, F., Huertas, E., García, C.M., 2008. Chlorophyll maxima and water mass interfaces: tidally induced dynamics in the Strait of Gibraltar. *Deep-Sea Res.* 155, 832–846 (doi).
- Marshall, J., Adcroft, A., Hill, C., Perelman, L., Heisey, C., 1997a. A finite-volume, incompressible Navier Stokes model for studies of the ocean on parallel computers. *J. Geophys. Res.* 102 (C3), 5753–5766. <http://dx.doi.org/10.1029/96JC02775>.
- Marshall, J., Hill, C., Perelman, L., Adcroft, A., 1997b. Hydrostatic, quasi-hydrostatic, and nonhydrostatic ocean modeling. *J. Geophys. Res.* 102 (C3), 5733–5752. <http://dx.doi.org/10.1029/96JC02776>.
- MEDAR Group, 2002. Medatlas 2002: Mediterranean and Black Sea Database of Temperature, Salinity and Bio-chemical Parameters Climatological Atlas. IFREMER Edition (4 Cdroms).
- Moum, J.N., Klymak, J.M., Nash, J.D., Perlin, A., Smith, W.D., 2007a. Energy transport by nonlinear internal waves. *J. Phys. Oceanogr.* 37, 1989–1988. <http://dx.doi.org/10.1175/JPO3094.1>.
- Moum, J.N., Farmer, D.M., Shroyer, E.L., Smith, W.D., Armi, L., 2007b. Dissipative losses in nonlinear internal waves propagating across the continental shelf. *J. Phys. Oceanogr.* 37, 1989–1995. <http://dx.doi.org/10.1175/JPO3091.1>.
- Nash, J.D., Moum, J.N., 2005. River plumes as a source of large-amplitude internal waves in the coastal ocean. *Nature* 437, 400–403. <http://dx.doi.org/10.1038/nature03936>.
- Nielsen, M.H., Pratt, L., Helfrich, K., 2004. Mixing and entrainment in hydraulically driven stratified sill flows. *J. Fluid Mech.* 15, 415–443.
- Pacanowski, R.C., Philander, S.G.H., 1981. Parameterisation of vertical mixing in numerical models of tropical oceans. *J. Phys. Oceanogr.* 11, 1443–1451.
- Sánchez Garrido, J.C., García Lafuente, J., Criado Aldeanueva, F., Baquerizo, A., Sannino, G., 2008. Time-spatial variability observed in velocity of propagation of the internal bore in the Strait of Gibraltar. *J. Geophys. Res.* 113, C07034. <http://dx.doi.org/10.1029/2007JC004624>.
- Sánchez Román, A., García Lafuente, J., Delgado, J., Sánchez Garrido, J.C., Naranjo, C., 2012. Spatial and temporal variability of tidal flow in the Strait of Gibraltar. *J. Mar. Syst.* <http://dx.doi.org/10.1016/j.marsys.2012.02.011>.
- Sánchez-Garrido, J.C., Sannino, G., Liberti, L., García Lafuente, J., Pratt, L., 2011. Numerical modelling of three-dimensional stratified tidal flow over Camarinal Sill, Strait of Gibraltar. *J. Geophys. Res.* 116, C12026. <http://dx.doi.org/10.1029/2011JC007093>.
- Sánchez-Román, A., Sannino, G., García Lafuente, J., Carillo, A., Criado-Aldeanueva, F., 2009. Transport estimates at the western section of the Strait of Gibraltar: a combined experimental and numerical modeling study. *J. Geophys. Res.* 114, C06002. <http://dx.doi.org/10.1029/2008JC005023>.
- Sannino, G., Carillo, A., Artale, V., 2007. Three-layer view of transports and hydraulics in the Strait of Gibraltar: a three-dimensional model study. *J. Geophys. Res.* 112, C03010. <http://dx.doi.org/10.1029/2006JC003717>.
- Sannino, G., Pratt, L., Carillo, A., 2009. Hydraulic criticality of the exchange flow through the Strait of Gibraltar. *J. Phys. Oceanogr.* 39 (11), 2779–2799. <http://dx.doi.org/10.1175/2009JPO4075.1>.
- Sannino, G., Sanchez-Garrido, J.C., Liberti, L., Pratt, L., 2012. Exchange flow through the Strait of Gibraltar as simulated by a σ -coordinate hydrostatic model and a z -coordinate non-hydrostatic mode. In: Borzelli, E., G.L., Gačić, M., Malanotte-Rizzoli, P., Lionello, P. (Eds.), *The Mediterranean Sea: temporal variability and spatial patterns*. AGU Monograph Series. AGU, Washington, D. C.
- Sanz, J.L., Acosta, J., Esteras, M., Herranz, P., Palomo, C., Sandoval, N., 1991. Prospección geofísica del Estrecho de Gibraltar (resultados del programa Hércules 1980–1983). *Publicaciones Especiales. Instituto Español de Oceanografía, Madrid, Spain* (48 pp).
- Stashchuk, N., Vlasenko, V., 2009. Generation of internal waves by a supercritical stratified plume. *J. Geophys. Res.* 114, C01008. <http://dx.doi.org/10.1029/2008JC004851>.
- Vázquez, A., Bruno, M., Izquierdo, A., Macías, D., Ruiz-Cañavate, A., 2008. Meteorologically forced subinertial flows and internal wave generation at the main sill of the Strait of Gibraltar. *Deep-Sea Res.* 155, 1277–1283. <http://dx.doi.org/10.1016/j.dsr.2008.05.008>.
- Vázquez, A., Flecha, S., Bruno, M., Macías, D., Navarro, G., 2009. Internal waves and short scale distribution patterns of chlorophyll in the Strait of Gibraltar and Alborán Sea. *Geophys. Res. Lett.* 36, L23601. <http://dx.doi.org/10.1029/2009GL040959>.
- Vlasenko, V., Stashchuk, N., 2007. Three-dimensional shoaling of large-amplitude internal waves. *J. Geophys. Res.* 112, C11018. <http://dx.doi.org/10.1029/2007JC004107>.
- Vlasenko, V., Sánchez-Garrido, J.C., Stashchuk, N., García-Lafuente, J., Losada, M., 2009. Three-dimensional evolution of large amplitude internal waves in the Strait of Gibraltar. *J. Phys. Oceanogr.* 39, 2230–2246. <http://dx.doi.org/10.1175/2009JPO4007.1>.
- Watson, G., Robinson, I.S., 1990. A study of internal waves propagation in the Strait of Gibraltar using shore-based radar images. *J. Phys. Oceanogr.* 20, 374–395.
- Wesson, J., Gregg, M., 1994. Mixing at Camarinal sill in the Strait of Gibraltar. *J. Geophys. Res.* 99 (C5), 9847–9878. <http://dx.doi.org/10.1029/94JC00256>.